Front. Earth Sci. 2020, 14(3): 660–672
https://doi.org/10.1007/s11707-020-0828-y

RESEARCH ARTICLE

Developing a USLE cover and management factor (*C*) for forested regions of southern China

Conghui LI[1*], Lili LIN[1,2*], Zhenbang HAO[1,2], Christopher J. POST[3], Zhanghao CHEN[1,2], Jian LIU[1,2], Kunyong YU (✉)[1,2]

1 Fujian Agriculture and Forestry University, Fuzhou 350002, China
2 University Key Laboratory for Geomatics Technology and Optimized Resources Utilization in Fujian Province, Fuzhou 350002, China
3 Department of Forestry and Environmental Conservation, Clemson University, Clemson SC 29634, USA

Abstract The Universal Soil Loss Equation model is often used to improve soil resource conservation by monitoring and forecasting soil erosion. This study tested a novel method to determine the cover and management factor (*C*) of this model by coupling the leaf area index (*LAI*) and soil basal respiration (*SBR*) to more accurately estimate a soil erosion map for a typical region with red soil in Hetian, Fujian Province, China. The spatial distribution of the *LAI* was obtained using the normalized difference vegetation index and was consistent with the *LAI* observed in the field (R^2 = 0.66). The spatial distribution of the *SBR* was obtained using the Carnegie–Ames–Stanford Approach model and verified by soil respiration field observations (R^2 = 0.51). Correlation analyses and regression models suggested that the *LAI* and *SBR* could reasonably reflect the structure of the forest canopy and understory vegetation, respectively. Finally, the *C*-factor was reconstructed using the proposed forest vegetation structure factor (C_s), which considers the effect of the forest canopy and shrub and litter layers on reducing rainfall erosion. The feasibility of this new method was thoroughly verified using runoff plots (R^2 = 0.55). The results demonstrated that C_s may help local governments understand the vital role of the structure of the vegetation layer in limiting soil erosion and provide a more accurate large-scale quantification of the *C*-factor for soil erosion.

Keywords leaf area index, remote sensing, soil basal respiration, forest vegetation structure factor, vegetation layer structure

Received March 24, 2020; accepted July 26, 2020

E-mail: yuyky@fafu.edu.cn

*The authors contributed equally to this work.

1 Introduction

Applications of soil erosion models have greatly improved soil erosion monitoring and forecasting (Montgomery, 2007; Devatha et al., 2015). However, the accuracy of soil erosion simulation is still hindered by the input parameters of ecohydrological models. The Universal Soil Loss Equation (USLE) is the most widely used model for estimating regional soil erosion (Devatha et al., 2015; Feng et al., 2018). This model considers five factors (Renard, 1997) (Eq. (1)):

$$A = R \times K \times LS \times C \times P, \quad (1)$$

where A is average annual soil loss rate ($t \cdot ha^{-1} \cdot y^{-1}$), R is the rainfall erosivity factor ($MJ \cdot mm \cdot ha^{-1} \cdot h^{-1} \cdot y^{-1}$), K is the soil erodibility factor ($t \cdot ha \cdot h \cdot ha^{-1} \cdot MJ^{-1} \cdot mm^{-1}$), LS is the topography factor (unitless), P is the support practice factor (unitless), and C is the cover and management factor (unitless). The last of these (henceforth referred to as the *C*-factor) is defined as the ratio between soil loss from a given land surface under specific cover conditions and the corresponding loss from farmlands (Wischmeier and Smith, 1978). This index is an effective and sensitive indicator for assessing soil erosion (Risse et al., 1993; Benkobi et al., 1994). The application of the USLE in the forest rather than agricultural systems is limited because it does not accurately capture the complex forest landscape (Elliot, 2004; Zhang et al., 2011). Moreover, it may not be reliable because it reflects the effects of forest cover and management on erosion rates, which is related to forest structure.

The calculation of *C*-factor values based on runoff is only applied at small scales, but remote sensing methods enable a larger-scale application. Vegetation coverage has been used as an input variable to extract *C*-factor values over long time periods (Feng et al., 2018). However, this

method has the following limitations that must be considered. First, vegetation indices are inconsistent with forest coverage as they tend to overestimate the latter during the growing season and underestimate it during the senescence period (Cyr et al., 1995). Second, the spatial resolution of remote sensing images affects the interpretation of understory vegetation cover because vegetation indices cannot fully reflect vertical forest structures such as shrub and litter layers (Gelagay and Minale, 2016). For instance, Figs. 1(a) and 1(b) depict the same vegetation coverage; nevertheless, Fig. 1(b) illustrates a plot with no understory vegetation, which is conducive to soil erosion. In such cases, soil erosion can be identified at close range. However, it is difficult to determine soil erosion from a distance due to extensive disturbance from the forest canopy. In other words, greater vegetation coverage does not always represent a greater capacity for soil and water conservation. As such, remote sensing-derived vegetation coverage data rarely represent the entire vegetation layer structure (i.e., trees, shrubs, and litter) and are therefore not appropriate for *C*-factor calculation (Mohamadi and Kavian, 2015; Anache et al., 2017).

Vertical layers of forest vegetation reduce surface runoff erosion through two main mechanisms: 1) reducing kinetic energy and direct rainfall-induced erosion by slowing rainfall through the canopy and from tree trunks (Wang et al., 2016) and 2) buffering rainfall with the shrub and litter layers (Arar and Chenchouni, 2014; Liu et al., 2016). Many studies have focused on the effect of vegetation layer structure on *C*-factor value variations. For instance, Wen et al. (2010) proposed a stratified vegetation cover index to better represent the vegetation layer structure, and Feng et al. (2018) used remote sensing images from different seasons to extract vegetation indices (e.g., the normalized difference tillage index or normalized difference senescent vegetation index). These indices reflect the structure of the vegetation layer according to vegetation growth in different periods and enable *C*-factor estimation using the relationship between vegetation indices and runoff data. The *C*-factor values vary according to the vegetation layer structure, which changes with season and precipitation (Alexandridis et al., 2015). Moreover, evergreen plants in subtropical zones do not defoliate in winter, creating difficulties in the extraction of yellow wavelengths (e.g., for the normalized difference senescent vegetation index), and this limits the large-scale application of C-factor values. Therefore, this study hypothesized that coupling the leaf area index (*LAI*) and soil basal respiration (*SBR*) may lead to reasonably accurate *C*-factor value estimations with potential widespread applicability. The *LAI* is an important indicator of plant canopy structure and is highly correlated with soil erosion (Zhang et al., 2014a). It can reflect the structure, distribution density, and biomass of vegetation (Lin et al., 2013). On the other hand, soil respiration is an important indicator of soil microbial quantity and activity (Yu et al., 2014) and can, therefore, be used as an indicator of shrub and litter layer occurrence (Rey et al., 2002; Zhang et al., 2016; Park et al., 2018).

The aim of this study was to explore indices that could adequately identify forest canopy characteristics and alternative indicators that may influence the identifiable attributes of lower forest layers to estimate *C*-factor values and provide basic data for accurate estimates of large-scale soil erosion. Hetian Town (China) was used as a case study as it is a unique hilly region with red soil and serious soil erosion (Xu et al., 2019; Yao et al., 2019). The objectives of this study were to 1) describe the applicability and model construction of an *LAI*-based remote sensing inversion of the forest canopy, 2) use remote sensing to estimate *SBR* and its applicability as an understory vegetation indicator, and 3) calculate an applicable *C*-factor based on the *LAI* and *SBR*.

2 Materials and methods

2.1 Study area

Hetian Town (25°33′–26°48′ N, 116°18′–116°31′ E) is located in Changting County, Fujian Province, southern China (Fig. 2). It covers a total area of approximately 296.7 km^2 and has a subtropical monsoon climate characterized by an average annual temperature of 17.5°C–18.8°C. Annual rainfall data from 1952 to 1982 (obtained from the Fujian Meteorological Bureau) ranged from 1074 to 2522 mm, with an average of 1750.8 mm. Elevation is 300–500 m above sea level. The dominant vegetation layers include Masson pine (*Pinus massoniana*; tree layer), *Adinandra millettii* and *Lespedeza bicolor* (shrub layer), and *Dicranopteris dichotoma* (herb layer).

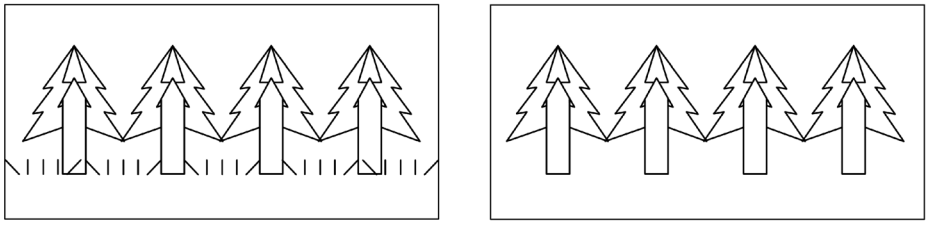

(a) (b)

Fig. 1 Schematic of a vegetation plot (a) with understory vegetation and (b) without understory vegetation.

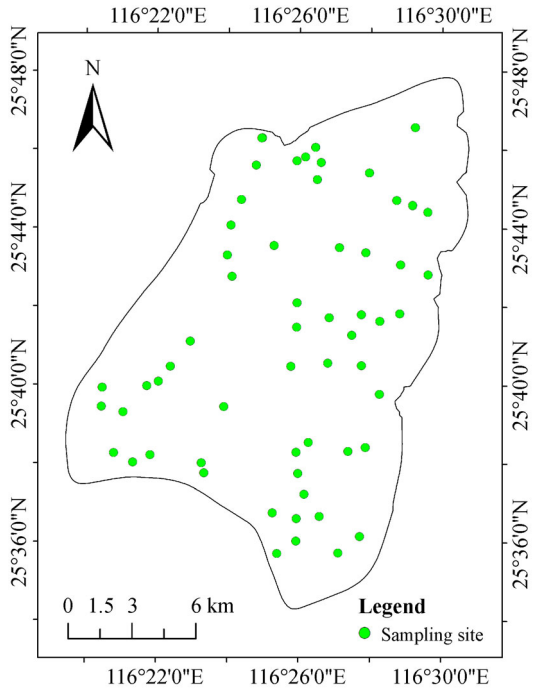

Fig. 2 Study area and location of the sampling plots.

The study area is a typical region with red soil subject to severe erosion caused by historical forest right disputes, large-scale deforestation, arson, and other anthropogenic factors (Lin et al., 2012; Chen et al., 2019). As reported by Lan (2012), as much as 96 km^2 of land was affected by soil erosion by the end of 2009. Consequently, Masson pine plantations exhibit poor growth rates of less than 20 cm/year in some areas, and no growth has been reported under some extreme local soil erosion conditions (Yuan et al., 2018; Yu et al., 2019).

2.2 Modeling

The USLE model, which is commonly used in China to estimate the *C*-factor values, is based on slope sediment yield data under natural and artificial rainfall, and can be described as follows (Cai et al., 2000):

$$\begin{cases} C = 1 & f_c = 0, \\ C = 0.6508 - 0.3436 \lg f_c & 0 < f_c < 78.3\%, \\ C = 0 & f_c \geqslant 78.3\%, \end{cases} \quad (2)$$

where f_c is the vegetation coverage and the *C*-factor is unitless and ranges from 0 to 1. This method cannot reflect the contributions of different vegetation layers and ignores the impact of understory vegetation and surface plant residues (litter layer) on runoff and sediment from hill slopes (Feng et al., 2018). Therefore, we propose the forest vegetation structure factor (C_s) (Lei and Wen, 2008) as an alternative to f_c to account for the vegetation layer structure as shown below:

$$C_s = aC_1 + (1-a)V_s, \quad (3)$$

where C_1 is the canopy structure factor determined from the *LAI* (see Section 2.2.1), V_s is the shrub and litter layer factor related to *SBR* (see Section 2.2.2), a is the weighting coefficient of soil and water conservation, C_1 and V_s reflect the coverage of trees and shrub and litter layers, respectively. Thus, the improved formula framework can be described as follows:

$$\begin{cases} C = 1 & C_s \leqslant X_1, \\ C = d + eC_s & X_1 < C_s < X_2, \\ C = 0 & C_s \geqslant X_2, \end{cases} \quad (4)$$

where X_1 and X_2 are the threshold values for C_s, and d and e are parameters. A flowchart of the overall method is shown in Fig. 3.

2.2.1 Construction of the canopy structure factor

The *LAI* is considered an important indicator for characterizing the forest canopy structure, and describing the ability of the canopy to intercept rainfall (Arora, 2002; Wang et al., 2014; Chen et al., 2019). Lin et al. (2013) proposed that the *LAI* replace vegetation coverage to estimate the *C*-factor via remote sensing. This index can more accurately represent the vegetation distribution (Wang et al., 2014; Ma et al., 2016) and thus resolve the limitations of two-dimensional remote sensing images.

The most common inversion model for the *LAI* using remote sensing was established from linear or nonlinear estimation models between the *LAI* and vegetation indices (Xie et al., 2018). Vegetation indices constitute a simple and effective way to express information pertaining to different vegetation states (Kang et al., 2016; Xie et al., 2018). Therefore, several vegetation indices (e.g., the atmospheric resistant vegetation index (*ARVI*), difference vegetation index (*DVI*), green normalized differential vegetation (*GNDVI*), modified soil-adjusted vegetation index (*MSAVI*), normalized differential vegetation index (*NDVI*), plant senescence reflectance index (*PSRI*), perpendicular vegetation index (*PVI*), re-normalized differential vegetation index (*RDVI*), ratio vegetation index (*RVI*), and soil-adjusted vegetation index (*SAVI*)) were selected based on their ability to express vegetation growth characteristics. These were compared with the *LAI* to construct correlation models as indicators of the forest canopy structure.

2.2.2 Construction of the shrub and litter layer factor

Shrub and litter layers are significantly correlated with the soil organic carbon content, soil temperature, and soil cover type (Jewell et al., 2017). Soil respiration is also

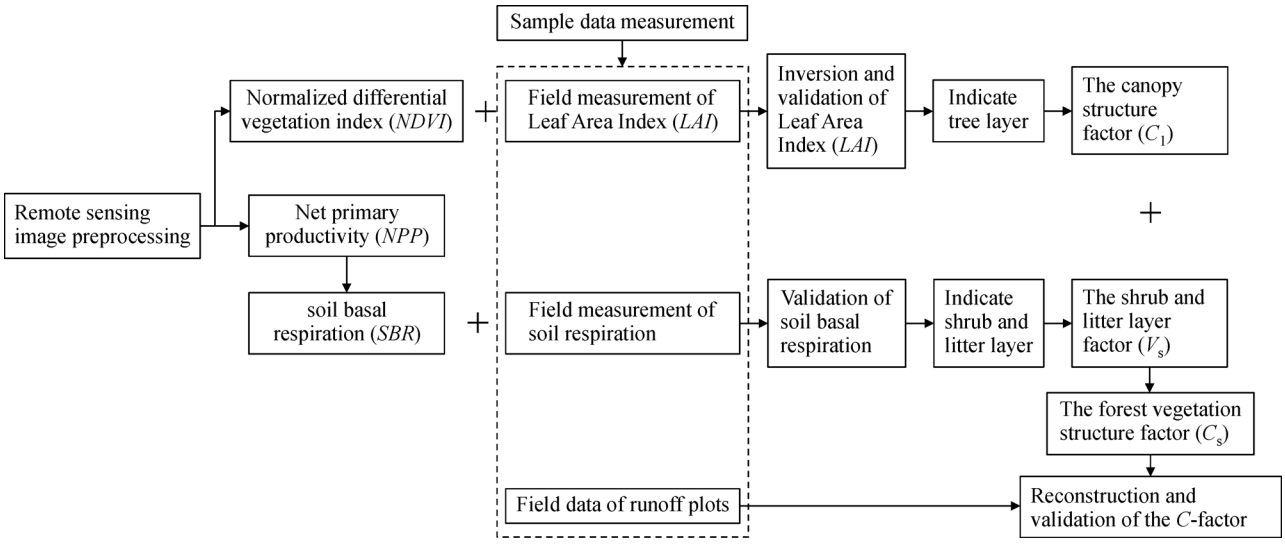

Fig. 3 Flowchart of the method to determine the proposed *C*-factor.

affected by the soil organic carbon content, moisture, and land cover type (Vose and Bolstad, 2007; Hursh et al., 2017; Yu et al., 2019). Therefore, understory vegetation and soil respiration are expected to be correlated (Rey et al., 2002; Park et al., 2018). A shrub and litter layer (V_s) factor was thus constructed via the following steps: 1) soil respiration inversion, 2) application of soil respiration to understory vegetation, and 3) construction of the V_s factor based on *SBR*.

Soil respiration is affected by soil temperature and moisture content (Qi et al., 2002; Rey et al., 2002; Wang et al., 2017); the relationship between soil respiration and understory vegetation may, therefore, depend on environmental factors. *SBR* is defined as the soil respiration value at 0°C under no water stress (Luo et al., 2001). The *SBR* inversion was obtained to eliminate the effect of soil temperature and soil moisture on soil respiration.

Net primary productivity (*NPP*) is largely influenced by the microbial characteristics of the soil (Raza and Mahmood, 2018) and indicates the removal of carbon dioxide from the air. *SBR* inversion is conducted using the NPP, which is estimated by the widely used Carnegie–Ames–Stanford approach (CASA) (Zhang et al., 2014b; Tripathi et al., 2018). This model is based on photosynthesis and considers vegetation characteristics and many aspects of vegetation under natural environmental conditions (Tripathi et al., 2018). Organic carbon is formed when litter enters the soil and is released when soil respiration occurs during vegetation growth, whereby carbon gradually reaches a dynamic equilibrium state. Therefore, the *NPP* carbon cycle model was used to estimate the monthly *SBR*, and the relationship between the estimated *SBR* and the understory was analyzed. A flow chart of the *NPP* estimation method based on the CASA is illustrated in Fig. 4.

The improved CENTURY model proposed by Zhou et al. (2007) was used to estimate the monthly *SBR* of the study site as follows:

$$SBR = \frac{NPP}{e^{\beta \times T} \times y}, \tag{5}$$

$$y = \frac{1}{1 + 30 \times e^{-8.5x}}, \tag{6}$$

$$x = \frac{PPT}{PET}, \tag{7}$$

$$Q_{10} = e^{10\beta}, \tag{8}$$

where *SBR* is the total amount of soil basal respiration derived from a monthly remote sensing-based NPP estimation ($gC \cdot m^{-2} \cdot month^{-1}$), y is the limiting factor of water on soil respiration, β is the temperature reaction coefficient, T is the temperature (°C), *PPT* is the monthly regional precipitation (mm), *PET* is the monthly potential evapotranspiration (mm), β has a value of 0.0794 (determined from the relationship between temperature and soil respiration measured in the field), Q_{10} has a value of 1.0826 in this study according to Eq. (8).

Given that the units of soil respiration from the remote sensing estimation (*SBR*) and field measurements differed, these values were converted into the same unit as follows:

$$SBR = R_0 \times 12 \times 3600 \times 24 \times 30 \times 10^{-6}, \tag{9}$$

$$R_s = R_0 e^{\beta T}, \tag{10}$$

where R_0 is the soil respiration rate at a reference temperature of 0°C ($\mu mol \cdot m^{-2} \cdot s^{-1}$), and R_s is the soil

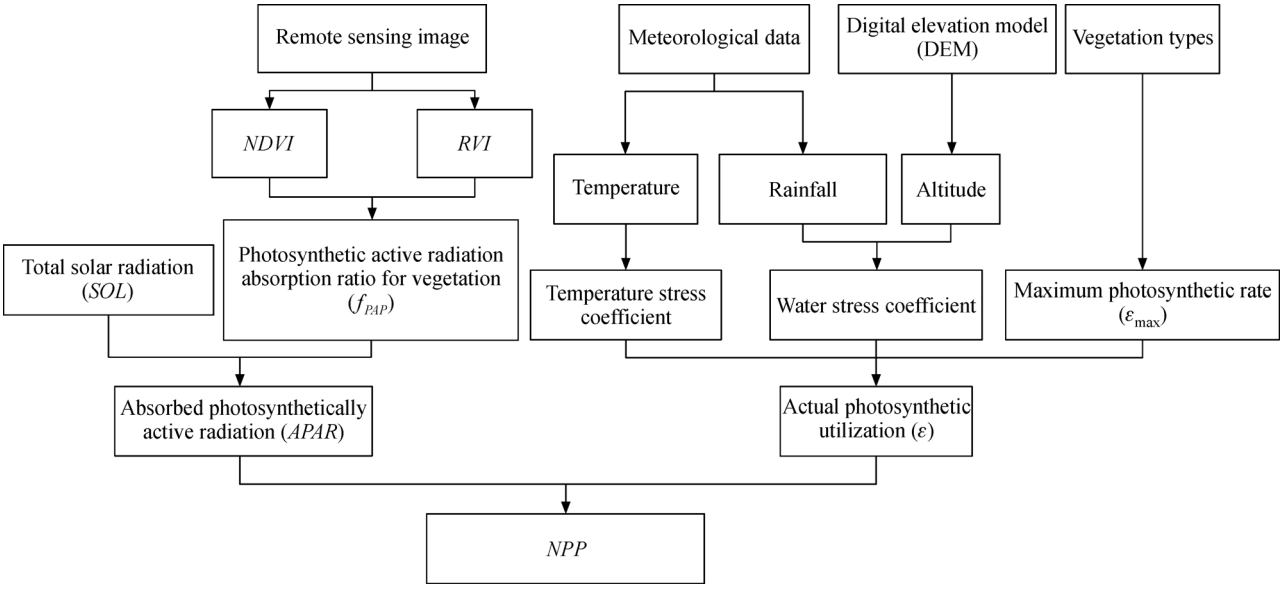

Fig. 4 Flowchart of net primary productivity estimation.

respiration rate ($\mu mol \cdot m^{-2} \cdot s^{-1}$). The constant 12 is the molar mass of *C* (12 $g \cdot mol^{-1}$), and the constants 3600, 24, and 30 represent the seconds in an hour, hours in a day, and days in a month, respectively. The number 10^{-6} is the micromole to mole conversion factor (1 μmol = 10^{-6} mol).

2.3 Preparation of data

Fieldwork was conducted in January 2015. A total of 59 plots (25.82 m × 25.82 m) were established in a Masson pine forest (Fig. 2). The soil respiration, *LAI*, shrub layer coverage, and litter layer thickness were measured in each. A description of study data are given in Table 1.

2.3.1 Remote sensing images and topographic data

Two images from the Pleiades satellite (France) were acquired on December 10, 2014 (view number: 0719-04222 and 0519-03996) and processed using the software ENVI 5.3 (Exelis VIS, USA). The processing included radiation and geometric correction and image mosaicking and clipping. The image was generated at a spatial resolution of 2 m.

Meteorological data including the mean monthly temperature and precipitation in, December 2014 and, January 2015, and multi-year mean precipitation from 1980 to 2010 were acquired from the Changting County Meteorological Bureau. All meteorological data were processed using the spatial statistics module in ArcGIS. The administrative boundary vector shape was also obtained.

2.3.2 Field measurement of soil respiration

Three PVC rings (inside diameter: 20 cm; height: 10 cm) were installed in each plot and were inserted 6 cm into the soil. Once the PVC rings were deployed, surface vegetation within the PVC rings was cut at least one day prior to measurement to ensure that air inside the soil within the rings stabilized.

Table 1 Description of study data

Data set	Description	Data source
Pleiades satellite images	December 10, 2014; 2 m spatial resolution multispectral data and 0.5 m spatial resolution panchromatic data; view number 0719-04222 and 0519-03996	France (available at L3Harris Geospatial website)
Meteorological data	Data were used to calculate net primary productivity, including mean monthly temperature, precipitation, multi-year mean precipitation, and solar radiation	Changting County Meteorological Bureau
Soil respiration	Measured by Li-8100A Carbon Flux Automatic Measurement System (LiCOR, USA) and used to verify the soil basl respiration inversion	Field survey
Leaf area index	Measured by LAI-2200 plant canopy analyzer (PCA, USA) and used to verify *LAI* inversion	Field survey
Runoff plot data	Observation data from runoff plots in Weifang watershed	Fujian Soil and Water Conservation Monitoring Station

A Li-8100A carbon flux automatic measurement system (LiCOR, USA) was used to measure soil respiration through the soil rings. All soil respiration measurements were taken between 09:00 and 16:00 LST. Each measurement was taken three times, nine for each plot, and the mean was taken as the soil respiration value. Soil temperature and moisture were obtained simultaneously with an internal Li-8100A soil temperature probe and a 10 cm soil moisture probe.

2.3.3 Vegetation data

The *LAI* was measured with an LAI-2200 plant canopy analyzer (PCA, USA), which automatically recorded the LAI value after the measurements were completed. When the LAI was determined, an initial value was measured in a clearing as a blank/reference value, and subsequent values were measured three times in the sample areas. The measurements were then repeated three times for each sample plot and the mean value was taken as the *LAI* value for each plot.

The vegetation parameters measured were forest canopy density, shrub layer coverage, and litter layer thickness. The shrub layer coverage was measured in 2 m × 2 m quadrats at a distance of 0.5 m from the center of the PVC ring, and litter layer thickness was measured in 1 m × 1 m quadrats at a 0.5 m distance from the center of the PVC ring. The average of three surveys was taken as the litter layer thickness. The litter layer coverage was considered to be 100% when the average litter layer thickness exceeded 3 cm (Lei and Wen, 2008).

2.3.4 Model validation

The collected data were divided into 40 modeling sets and 19 testing sets. The coefficient of determination (R^2) was used to evaluate the precision of the estimation model; higher R^2 values indicated a stronger correlation with the field measurements. Moreover, the root-mean-square error (*RMSE*), mean relative accuracy (*MRA*), and mean estimation accuracy (*MEA*) were calculated as follows, to assess the model accuracy:

$$RMSE = \sqrt{\frac{1}{n}\sum_{i=1}^{n}(y_i - \hat{y}_i)^2}, \tag{11}$$

$$MRA = \frac{1}{n}\sum_{i=1}^{n}\left(1 - \frac{|y_i - \hat{y}_i|}{y_i} \times 100\%\right), \tag{12}$$

$$MEA = 1 - \frac{|\sum_{i=1}^{n} y_i - \sum_{i=1}^{n} \hat{y}_i|}{\sum_{i=1}^{n} y_i} \times 100\%, \tag{13}$$

where $\hat{y}_i$ is the measured value of sample i, y_i is the estimated value of sample i,, n is the total number of samples.

The determination of the soil and water conservation coefficient at different vertical layers is key to constructing the C_s. In this study, the soil and water conservation coefficient at different levels of the vertical structure were determined via observations of 12 runoff plots in the Weifang watershed, Hetian (Table 2). The average canopy closure of the runoff plots was 0.6, the average shrub layer coverage was 80%, and the litter layer thickness was 3 cm. Runoff measurement data were used to verify the estimation of the *C*-factor values; these were obtained from the Fujian Soil and Water Conservation Monitoring Station.

Furthermore, the soil erodibility factor (*K*) in the USLE model is often set to 0.22 for a typical hilly area with red soil (Liu, 2006), as follows:

$$C = y/y_{st}, \tag{14}$$

$$y_{st} = 100K, \tag{15}$$

where y_{st} is the y value under standard conditions.

Based on slope sediment yield data under natural rainfall in the study plots, the relationship between C_s and the sediment yield on the slope was analyzed using the following model:

$$y = 76.939 - 17.8\ln C_s \ (R^2 = 0.638,\ n = 12), \tag{16}$$

where y is the sediment yield per unit area (g/m^2).

3 Results

3.1 Leaf area index inversion results and accuracy analysis

To determine which of the linear, logarithmic, quadratic, power, and exponential regression models achieved the best fit, field *LAI* data from 59 samples were tested against the *ARVI*, *DVI*, *GNDVI*, *MSAVI*, *NDVI*, *PSRI*, *PVI*, *RDVI*, *RVI*, and *SAVI*. The power model with *NDVI* provided the best *LAI* inversion model (R^2 = 0.66; *RMSE* = 0.59; *MRA* = 82.99%; *MEA* = 98.14%) (Table 3). Therefore, the *LAI* inversion for the study area was based on Eq. (17) (Fig. 5), which indicated the distribution of the *LAI*, as follows:

Table 2 Runoff depth observations in Weifang using different models

Model	Tree, shrub, and litter control model	Shrub and litter control model	Litter clearance model (shrub control model)	Farmland management model
Runoff depth/mm	81.4	89.1	123.7	142.4

Table 3 The best inversion results of leaf area index (*LAI*) in each model type

VI	Model type	Estimation model	Validation indicators			
			R^2	*RMSE*	*MRA*	*MEA*
RVI	Linear	$y = 0.983x - 0.594$	0.63	0.51	78.83%	96.37%
RVI	Logarithmic	$y = 3.289\ln x - 1.255$	0.62	0.57	81.35%	97.85%
RVI	Quadratic	$y = -0.005x^2 + 0.977x - 0.661$	0.63	0.51	78.97%	96.37%
NDVI	Power	$y = 7.895x^{1.791}$	0.66	0.59	82.99%	98.14%
NDVI	Exponential	$y = 0.351e^{3.656x}$	0.65	0.52	82.48%	99.66%

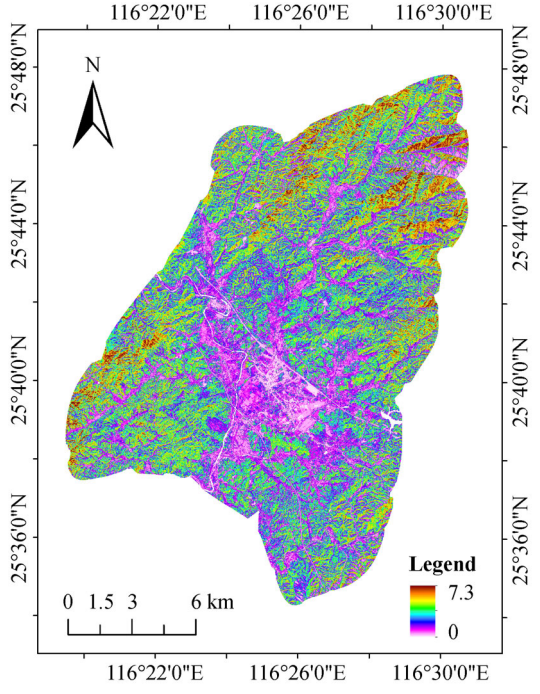

Fig. 5 Distribution of leaf area index.

$$LAI = 7.895x^{1.791}. \quad (17)$$

3.2 Soil basal respiration inversion results and accuracy analysis

The *NPP* of the study area was spatially estimated using CASA parameters. The average *NPP* distribution during January 2015 was 18.43 $gC \cdot m^{-2} \cdot month^{-1}$ (Fig. 6(a)). Based on this, the spatial distribution of *SBR* had an average value of 10.17 $gC \cdot m^{-2} \cdot month^{-1}$ (Fig. 6(b)). The accuracy of the *SBR* was verified using soil respiration measurement values, with the units transformed according to Eq. (9). The resulting model had an R^2 value of 0.51, *MRA* of 77.83%, and *MEA* of 97.27% (Fig. 7). The soil respiration measurement rate varied between 0.37 and 1.76 $\mu mol \cdot m^{-2} \cdot s^{-1}$, with an average of 0.95 $umol \cdot m^{-2} \cdot s^{-1}$. Additionally, the estimated soil respiration rate was 0.45–1.82 $\mu mol \cdot m^{-2} \cdot s^{-1}$ with an average of 0.92 $\mu mol \cdot m^{-2} \cdot s^{-1}$ (Table 4).

3.3 Applicability analysis of soil basal respiration compared to understory vegetation

The *SBR* was positively correlated with shrub layer coverage and litter layer thickness (Table 5), suggesting that *SBR* is a good indicator of these factors. Therefore, the shrub layer coverage and litter layer thickness were taken as independent variables and *SBR* was taken as the dependent variable to construct the linear, logarithmic, quadratic, power, and exponential function models. These models were verified using the measured sample data. In the fitted model of shrub layer coverage and *SBR*, *SBR* increased with both shrub layer coverage and litter layer thickness in all five regression models. According to the test data from the measured plots, the linear regression models of shrub layer coverage and SBR ($R^2 = 0.62$; *RMSE* = 1.67; *MRA* = 84.42%; *MEA* = 98.04%) and litter layer thickness and SBR (R^2 = 0.47; *RMSE* = 1.96; *MRA* = 84.39%; *MEA* = 97.31%) exhibited the best results (Table 6).

3.4 Reconstruction and verification of the cover and management factor

A farmland management model used as reference and the runoff plot results summarized in Table 2 indicated that the overall runoff reduction rates of the tree, shrub, and litter control model, shrub and litter control model, and litter clearance model (shrub control model) were 42.84, 37.43, and 13.13%, respectively (Table 7). Thus, C_s and V_s were expressed as follows:

Table 4 Accuracy evaluation of soil respiration (R_s) model for Masson pine plantations

Forest type	Sample (*n*)	Measured R_s /($\mu mol \cdot m^{-2} \cdot s^{-1}$)			Estimated R_s /($\mu mol \cdot m^{-2} \cdot s^{-1}$)			*MRA*	*MEA*
		Min	Mean	Max	Min	Mean	Max		
Masson pine	59	0.37	0.95	1.76	0.45	0.92	1.82	77.83%	97.27%

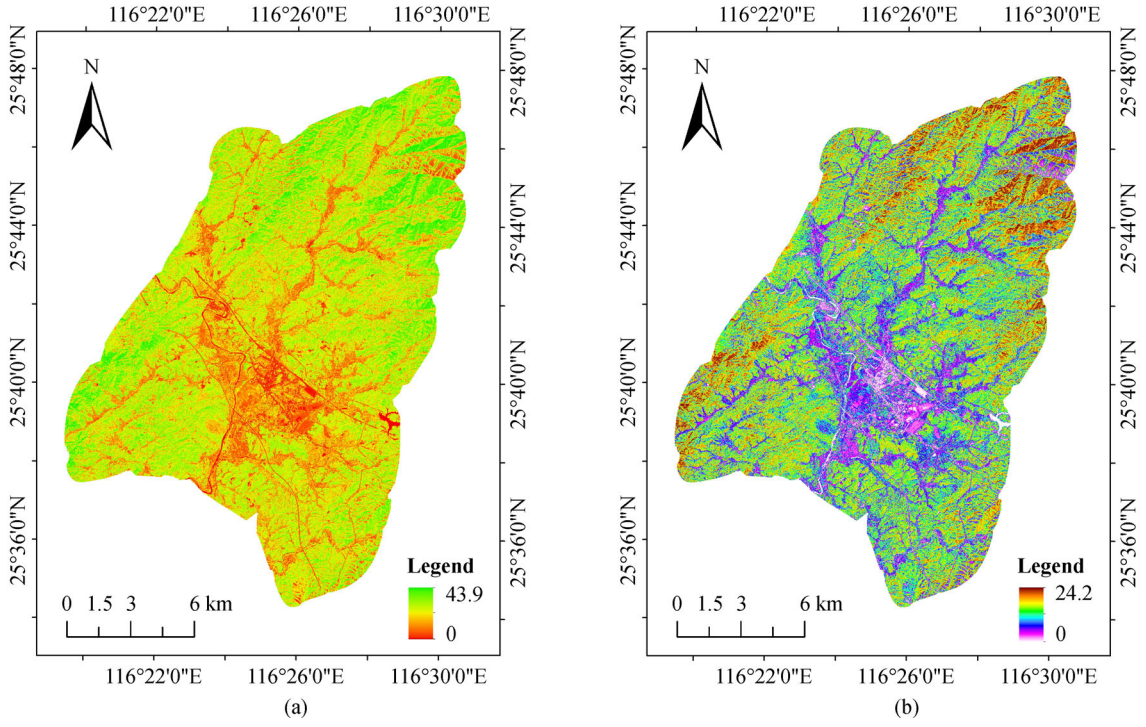

Fig. 6 (a) Net primary productivity (*NPP*) distribution and (b) soil basal respiration (*SBR*) distribution.

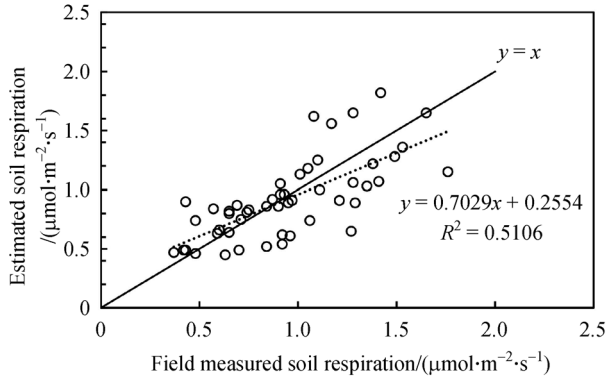

Fig. 7 Comparison of measured and estimated soil respiration rates ($\mu mol \cdot m^{-2} \cdot s^{-1}$).

Table 5 Correlations between litter layer thickness (*LLT*), understory vegetation coverage (*UVC*), and soil basal respiration (*SBR*)

Factor	*LLT*	*UVC*	*SBR*
LLT	1	0.457**	0.527**
UVC	–	1	0.729**
SBR	–	–	1

Note: ** $P < 0.01$.

$$C_s = 0.181C_1 + 0.819V_s. \quad (18)$$

The relationship between C_s and the *C*-factor was obtained by combining C_s and the sediment yield in the slope (Eq. (16)). Considering that the *C*-factor value ranged from 0 to 1, the *C*-factor in Hetian was summarized as follows:

Table 6 Assessment of models for litter layer thickness (*LLT*) and understory vegetation coverage (*UVC*)

Factor	Best-fit model	*RMSE*	*MRA*	*MEA*
UVC	$y = 0.173x + 7.440$	1.67	84.42%	98.04%
LLT	$y = 1.294 + 6.925$	1.96	84.39%	97.31%

Table 7 Weights of forest vertical structure

Item	Tree	Shrub and grass	Litter
Reduction ratio/%	5.41	13.13	24.30
Reduction flow coefficient of unit coverage	0.090	0.164	0.243
Weight	0.181	0.330	0.489

$$\begin{cases} C = 1 & C_s \leqslant 21.90\%, \\ C = 3.497 - 0.809\ \ln C_s & 21.90\% < C_s < 75.39\%, \\ C = 0 & C_s \geqslant 75.39\%. \end{cases} \quad (19)$$

In this study, C_s was determined using the *LAI* and *SBR*. Thus, the correlation between the measured the *LAI* and canopy closure of the plots was analyzed as follows:

$$C_1 = 16.36LAI + 14.18 \ \ (R^2 = 0.7584,\ n = 54). \quad (20)$$

The value of V_s based on the linear relationship between the *SBR* and shrub and litter layer coverage was determined as follows:

$$V_s = 2.825SBR - 20.791. \quad (21)$$

A C_s spatial distribution map was constructed based on the inversion of the *LAI* and *SBR* (Fig. 8). Finally, the accuracy of the reconstructed *C*-factor simulated data were verified using the measured data from the runoff plots (R^2 = 0.55) (Fig. 9). The calculation of the *C*-factor value in the Masson pine forest was 0.18.

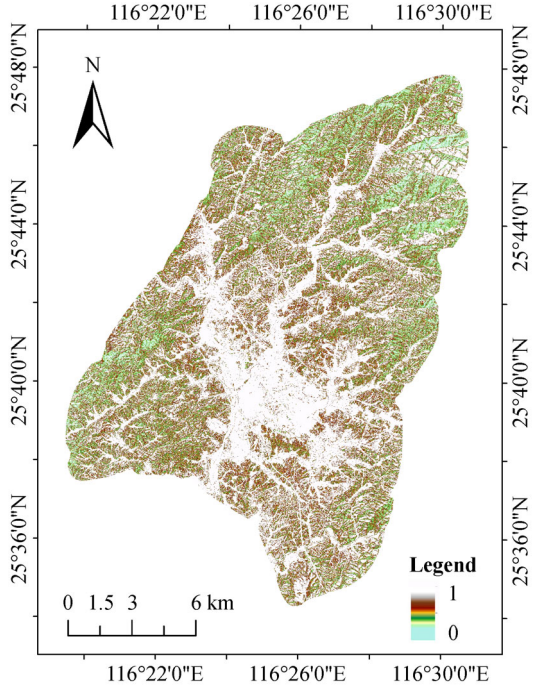

Fig. 8 C-factor map determined from leaf area index (*LAI*) and soil basal respiration (*SBR*).

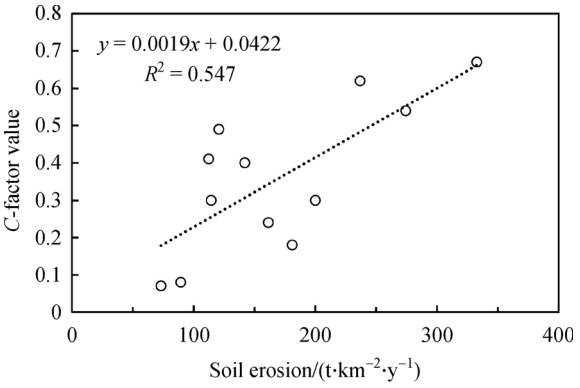

Fig. 9 Relationship between *C*-factor and soil erosion in study area.

4 Discussion

4.1 *C*-factor estimation based on different factors

The *C*-factor estimations between the *C*-factor and vegetation cover are widely applied in the world. Thus, we used the most common vegetation index (*NDVI*) (Wen et al., 2010) and *LAI* (Lin et al., 2013), as vegetation cover respectively to calculate the *C*-factor in Hetian based on the *C*-factor calculation method of Cai et al. (2000). The relationship between vegetation cover and the *C*-factor was determined via field observations of runoff subsidence sediment yields on a slope affected by natural rainfall in the Weifang watershed:

$$y = 46.595 - 10.5\ln f_c \ \ (R^2 = 0.6867, n = 12), \quad (22)$$

where y is the slope sediment yield per unit area ($g \cdot m^{-2}$), and f_c is the vegetation coverage (%).

Figure 10 showed the *C*-factors was determined by *NDVI* and *LAI*, respectively. Additionally, the data measured from the runoff plots were used for verification. The *C*-factor estimated by vegetation coverage in the study area was similar to that determined in the previous studies (Cai et al., 2000). Nevertheless, the *C*-factor model based on *NDVI* extracted by the Pleiades satellite image only reflected the projected vegetation cover and the results were weak (R^2 = 0.36). The *C*-factor based on the *LAI* accounted for the characteristics of the vegetation structure relatively well (R^2 = 0.53) (Fig. 11), but did not consider plant residue such as litter. The *C*-factor could potentially bias some soil erosion assessment models and neglect the role that different vegetation layers play in controlling soil erosion (Mohamadi and Kavian, 2015; Anache et al., 2017). Notably, the *C*-factor model based on the *LAI* and *SBR* — and which considered the canopy, shrub and litter layers — produced the highest R^2 value. Moreover, compared with the developing *C*-factor value based on vegetation cover, the proposed *C*-factor estimated higher soil erosion intensity. This was closely related to the low soil fertility and minimal understory vegetation in Hetian.

4.2 Comparison with other validation studies

The results of this study were compared with those of other studies. The R^2 values show that developing the *C*-factor

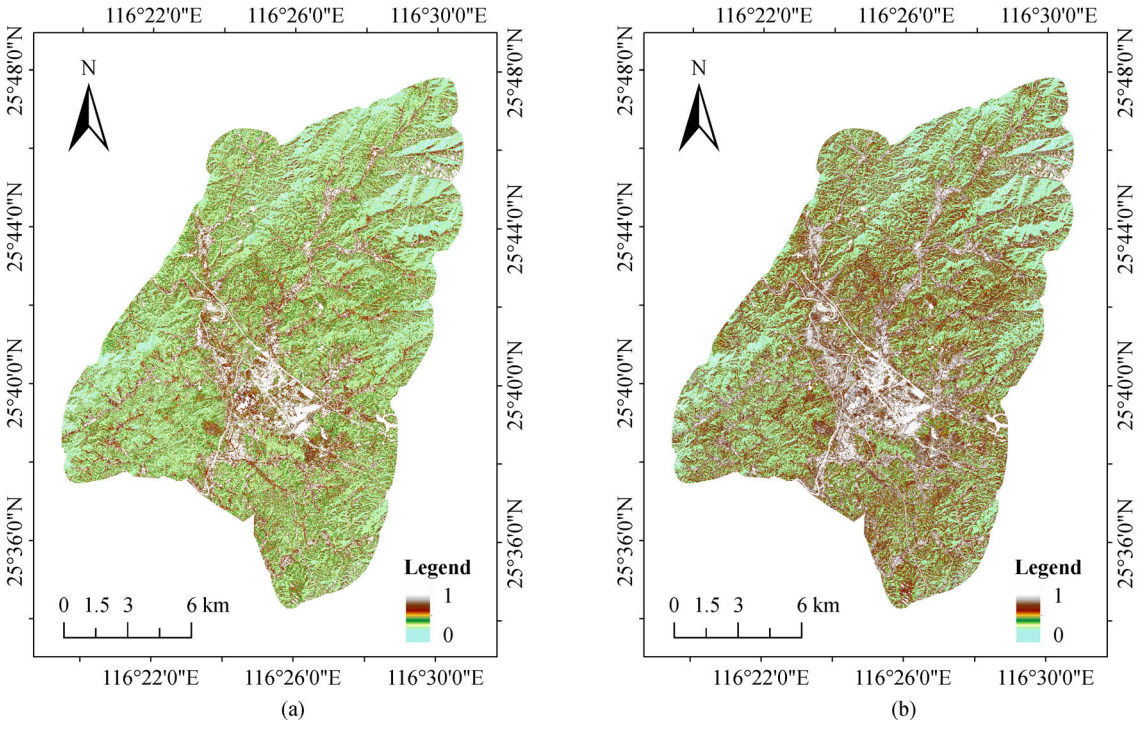

Fig. 10 *C*-factor map based on (a) Normalized difference vegetation index (*NDVI*) and (b) Leaf area index (*LAI*).

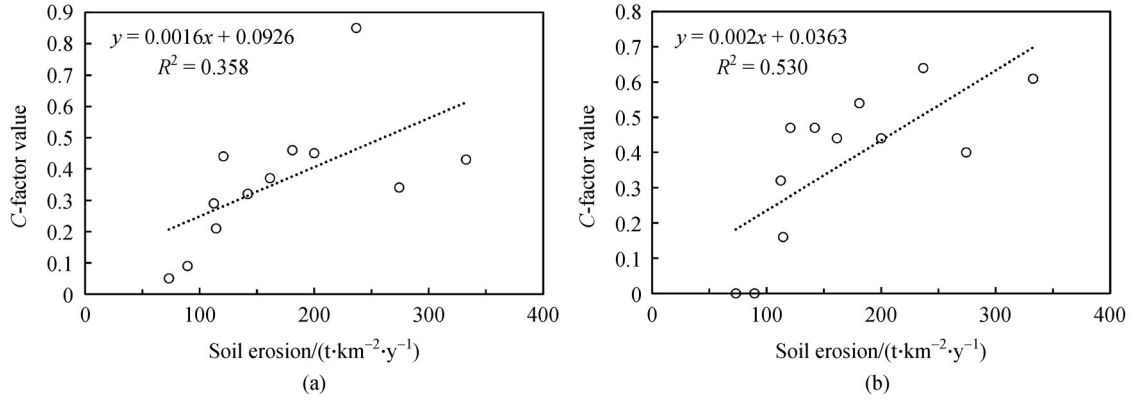

Fig. 11 Relationship between soil erosion and *C*-factor determined by (a) Normalized difference vegetation index (*NDVI*) and (b) Leaf area index (*LAI*).

Table 8 Validation of the relationship equations between the *C*-factor and vegetation coverage

References	Relationship equations	Validation at Weifang watershed R^2
Bu et al. (1993)	$C = 0.450 - 0.00786\, f_c$	0.423
Jiang et al. (1996)	$C = \exp[-0.0085(f_c - 5)^{1.5}]$; $f_c > 5\%$ $C = 1$; $f_c \leqslant 5\%$	0.269
Cai et al. (2000)	$C = 1$; $f_c = 0$ $C = 0.6508 - 0.3436 \lg f_c$; $0 < f_c < 78.3\%$ $C = 0$; $f_c \geqslant 78.3\%$	0.483
Jiang (2005)	$C = 1$; $f_c = 0$ $C = 0.6665 - 0.3436 \lg f_c$; $0 < f_c < 87\%$ $C = 0$; $f_c > 87\%$	0.359

using the *LAI* and *SBR* was better than using vegetation cover (Table 8). Previous studies developed equations for determining the *C*-factor that could be used to calculate the *C*-factor in Hetian (Bu et al., 1993; Jiang et al., 1996; Cai et al., 2000; Jiang, 2005); relationships between vegetation coverage and *C*-factor in the Weifang watershed, Hetian, were also established. The accuracy of these models was validated using observed runoff soil erosion data.

The observed soil erosion in the Weifang watershed had a lower R^2 value when estimated using the equation in Jiang et al. (1996), which indicated that this equation should be revised when used for other regions. The calculation of the *C*-factor values via the equation in Bu et al. (1993) yielded some negative values, which were out of range, despite the moderate R^2 value. The *C*-factor equation proposed by Jiang (2005) was applied to Changting but did not yield satisfactory results for Hetian. The *C*-factor estimated by Cai et al. (2000) had a better relationship with soil erosion than others in Hetian. This indicates that it is appropriate to couple the *LAI* and *SBR* to develop the *C*-factor by adjusting the equation in Cai et al. (2000). A lower R^2 value indicated that the model was not suitable for estimating the *C*-factor in Hetian. Overall, the estimation of *C*-factor values from these equations was no better than that using C_s.

4.3 Accuracy of the proposed *C*-factor parameters

In this study, remote sensing data with a high spatial resolution were used to estimate the *C*-factor and obtain an accurate value for it. The results showed that *NDVI* can adequately represent the spatial distribution of *LAI* (R^2 = 0.66), which is consistent with previous studies that showed that vegetation indices obtained from remote sensing images can effectively represent the *LAI* distribution (Jiao et al., 2014). Moreover, it revealed the relationships between *SBR* and understory vegetation in a manner that accounted for the role of *SBR*. The results can most likely be explained by the mechanisms outlined in previous studies, e.g., the interception of rainfall in the forest canopy significantly reduces direct erosion (Mohamadi and Kavian, 2015) and understory vegetation reduces surface runoff (Anache et al., 2017).

The correlation analysis of *SBR* and measured soil respiration indicated that the estimated *SBR* rate reflected the field soil respiration rate in the study area and indirectly supported the reliability of *NPP* and *SBR* results derived from remote sensing data. Models driven by remote sensing data are widely used and accepted for indirect *NPP* estimation (Ricotta et al., 1999). Although the spatiotemporal variation of *NPP* is affected by a combination of various factors, the *NPP* produced by the CASA model and various meteorological parameters is fairly comprehensive because it considers vegetation growth conditions. *NPP* values for the study area were consistent with Zheng et al. (2008) for another hilly area with red soil and other measured *NPP* ranges (Liu et al., 1998).

Uncertainties concerning the combination of remote sensing images, the CASA model, and soil respiration field measurements remain. They are related to inconsistent spatial data scales (Turner et al., 2005) and zonal factors such as soil parent material, which may influence soil respiration (Trumbore et al., 2006). The temperature sensitivity factor (Q_{10}) is the most sensitive index when estimating the *SBR*. It is important for simulating the feedback intensity between global climate change and the amount of carbon released from an ecosystem. The Q_{10} value has significant spatial heterogeneity resulting from geographical location, seasonal conditions, and ecosystem types (Qi et al., 2002; Wang et al., 2017). Zhou et al. (2007) proposed that the average Q_{10} value is 1.80 in China, and the range of Q_{10} for different soil types vary between 1.09 and 2.38. In this study, Q_{10} was calculated by measuring the response of soil respiration to temperature. It is the most commonly used method for estimating Q_{10} in the inversion of *SBR* (Larsen and MacDonald, 2007; Feng et al., 2008). Compared with the results of Zhou et al. (2007), the Q_{10} value was within a reasonable range. Generally, the controller of the Q_{10} value improved the simulation of SBR.

5 Conclusions

The accuracy of the *C*-factor is directly related to that of soil erosion estimation results. In this study, C_s was used to explain the effect of different vegetation layers on soil erosion during rainfall, to better understand and ultimately reduce rainfall-induced erosion. The combination of the *LAI* and *SBR* enabled simultaneous analysis of three-dimensional data above the ground and two-dimensional data on the surface. The results showed that the reconstructed *C*-factor coupled with the *LAI* and *SBR* is feasible and accurate. Using this approach, the *C*-factor can best reflect the vegetation layer structure and is useful to comprehensively and accurately quantify large-scale soil erosion.

Acknowledgements This work was supported by the National Natural Science Foundation of China (Grant Nos. 31770760 and 41401385) and the scholarship program of China Scholarship Council (No. 201908350124).The authors wish to thank Ping He, Suping Yang, Dejin Xie, Jinzhao Zhang, Wenying Zheng, Qi Zeng, Shayi ShangGuan, Jingwen Ai, and Tongzhou Lin for their assistance in the field investigations and experiments.

References

Alexandridis T K, Sotiropoulou A M, Bilas G, Karapetsas N, Silleos N G (2015). The effects of seasonality in estimating the *C*-factor of soil erosion studies. Land Degrad Dev, 26(6): 596–603

Anache J A, Wendland E C, Oliveira P T, Flanagan D C, Nearing M A (2017). Runoff and soil erosion plot-scale studies under natural

rainfall: a meta-analysis of the Brazilian experience. Catena, 152: 29–39

Arar A, Chenchouni H (2014). A "simple" geomatics-based approach for assessing water erosion hazard at montane areas. Arab J Geosci, 7(1): 1–12

Arora V (2002). Modeling vegetation as a dynamic component in soil–vegetation–atmosphere transfer schemes and hydrological models. Rev Geophys, 40(2): 1–26

Benkobi L, Trlica M J, Smith J L (1994). Evaluation of a refined surface cover subfactor for use in RUSLE. Rangeland Ecol Manag, 47(1): 74–78

Bu Z H, Zhao H F, Liu S Q, Chen M H (1993). Preliminary study on algorithm formula of vegetative factor for undisturbed areas in remote sensing monitoring soil loss. Remote Sensing Technology and Application, 8(4): 16–22 (in Chinese)

Cai C F, Ding S W, Shi Z H, Huang L, Zhang G Y (2000). Study of applying USLE and geographical information system IDRISI to predict soil erosion in small watershed. J Soil Water Conserv, 14(2): 19–24 (in Chinese)

Chen S F, Zha X, Bai Y H, Wang L Y (2019). Evaluation of soil erosion vulnerability on the basis of exposure, sensitivity, and adaptive capacity: a case study in the Zhuxi watershed, Changting, Fujian Province, southern China. Catena, 177: 57–69

Cyr L, Bonn F, Pesant A (1995). Vegetation indices derived from remote sensing for an estimation of soil protection against water erosion. Ecol Modell, 79(1–3): 277–285

Devatha C P, Deshpande V, Renukaprasad M S (2015). Estimation of soil loss using USLE model for Kulhan Watershed, Chattisgarh—a case study. Aquatic Procedia, 4: 1429–1436

Elliot W J (2004). WEPP internet interfaces for forest erosion prediction. J Am Water Resour Assoc, 40(2): 299–309

Feng Q, Zhao W W, Ding J Y, Fang X N, Zhang X (2018). Estimation of the cover and management factor based on stratified coverage and remote sensing indices: a case study in the Loess Plateau of China. J Soils Sediments, 18(3): 775–790

Feng W T, Zou X M, Sha L Q, Chen J H, Feng Z L, Li J Z (2008). Comparisons between seasonal and diurnal patterns of soil respiration in a montane evergreen broad-leaved forest of Ailao mountains. J Plant Ecol, 32: 31–39 (in Chinese)

Gelagay H S, Minale A S (2016). Soil loss estimation using GIS and Remote sensing techniques: a case of Koga watershed, Northwestern Ethiopia. ISWCR, 4(2): 126–136

Hursh A, Ballantyne A, Cooper L, Maneta M, Kimball J, Watts J (2017). The sensitivity of soil respiration to soil temperature, moisture, and carbon supply at the global scale. Glob Change Biol, 23(5): 2090–2103

Jewell M D, Shipley B, Low-Décarie E, Tobner C M, Paquette A, Messier C, Reich P B (2017). Partitioning the effect of composition and diversity of tree communities on leaf litter decomposition and soil respiration. Oikos, 126(7): 959–971

Jiang H (2005). Soil erosion monitoring and eco-security evaluation on Changting. Dissertation for the Master's Degree. Fuzhou: Fuzhou University (in Chinese)

Jiang Z S, Wang Z Q, Liu Z (1996). Study on the use of GIS to estimate soil erosion in a small watershed in the loess hilly region. Research of Soil and Water Conservation, 3(2): 84–97 (in Chinese)

Jiao Z M, Zhang X L, Li F L, Shi K, Ning L L, Wang Y T, Zhao M Y (2014). Impact of multispectral bands texture on leaf area index using Landsat-8. Geography and Geo-Information Science, 30(3): 42–45 (in Chinese)

Kang Y, Özdoğan M, Zipper S C, Román M O, Walker J, Hong S Y, Marshall M, Magliulo V, Moreno J, Alonso L, Miyata A, Kimball B, Loheide S P (2016). How universal is the relationship between remotely sensed vegetation indices and crop leaf area index? A global assessment. Remote Sens (Basel), 8(7): 597

Lan L J (2012). Study on ecological restoration treatments of degraded red soil in Western Fujian Province. Dissertation for the Master's Degree. Fuzhou: Fujian Agriculture and Forestry University (in Chinese)

Larsen I J, MacDonald L H (2007). Predicting postfire sediment yields at the hillslope scale: testing RUSLE and disturbed WEPP. Water Resour Res, 43(11):W11412

Lei W N, Wen Z M (2008). Research on soil erosion vegetation factor index based on community structure. J Soil Water Conserv, 22(5): 68–72 (in Chinese)

Lin C, Zhou S L, Wu S H, Liao F Q (2012). Relationships between intensity gradation and evolution of soil erosion: a case study of Changting in Fujian Province, China. Pedosphere, 22(2): 243–253

Lin J, Zhang J C, Gu Z Y, Wu Y M (2013). Quantitative assessment of vegetation cover and management factor based on leaf area index and remote sensing. Sci Silva Sin, 49(2): 86–92 (in Chinese)

Liu H, Blagodatsky S, Giese M, Liu F, Xu J, Cadisch G (2016). Impact of herbicide application on soil erosion and induced carbon loss in a rubber plantation of southwest China. Catena, 145: 180–192

Liu J (2006). Study on the efficient spatial allocation of the ecological forest system in Minjiang watershed based on geomatics. Dissertation for the Doctoral Degree. Beijing: Beijing Forestry University (in Chinese)

Liu S R, Guo Q S, Wang B (1998). Prediction of net primary productivity of forests in China in response to climate change. Acta Ecol Sin, 18 (5): 478–483 (in Chinese)

Luo Y, Wan S, Hui D, Wallace L L (2001). Acclimatization of soil respiration to warming in a tall grass prairie. Nature, 413(6856): 622–625

Ma B, Li C D, Li Z B, Wu F Q (2016). Effects of crops on runoff and soil loss on sloping farmland under simulated rainfall. CLEAN–Soil Air Water, 44(7): 849–857

Mohamadi M A, Kavian A (2015). Effects of rainfall patterns on runoff and soil erosion in field plots. Int Soil Water Conserv Res, 3(4): 273–281

Montgomery D R (2007). Soil erosion and agricultural sustainability. Proc Natl Acad Sci USA, 104(33): 13268–13272

Park H, Lim S, Kwak J, Yang H, Lee K, Lee Y, Kim H, Choi W (2018). Elevated CO_2 concentration affected pine and oak litter chemistry and the respiration and microbial biomass of soils amended with these litters. Biol Fertil Soils, 54(5): 583–594

Qi Y, Xu M, Wu J G (2002). Temperature sensitivity of soil respiration and its effects on ecosystem carbon budget: nonlinearity begets surprises. Ecol Modell, 153(1–2): 131–142

Raza S M H, Mahmood S A (2018). Estimation of net rice production through improved CASA model by addition of soil suitability constant (ha). Sustainability, 10(6): 1788

Renard K G (1997). Predicting Soil Erosion by Water: A Guide to Conservation Planning with the Revised Universal Soil Loss Equation (RUSLE). Washington D.C: United States Government Printing

Rey A, Pegoraro E, Tedeschi V, De Parri I, Jarvis P G, Valentini R (2002). Annual variation in soil respiration and its components in a coppice oak forest in Central Italy. Glob Change Biol, 8(9): 851–866

Ricotta C, Avena G, De Palma A (1999). Mapping and monitoring net primary productivity with AVHRR *NDVI* time-series: statistical equivalence of cumulative vegetation indices. ISPRS J Photogram, 54(5–6): 325–331

Risse L M, Nearing M A, Laflen J M, Nicks A D (1993). Error assessment in the universal soil loss equation. Soil Sci Soc Am J, 57 (3): 825–833

Tripathi P, Patel N R, Kushwaha S P S (2018). Estimating net primary productivity in tropical forest plantations in India using satellite-driven ecosystem model. Geocarto Int, 33(9): 988–999

Trumbore S, Da Costa E S, Nepstad D C, Barbosa De Camargo P, Martinelli L A, Ray D, Restom T, Silver W (2006). Dynamics of fine root carbon in Amazonian tropical ecosystems and the contribution of roots to soil respiration. Glob Change Biol, 12(2): 217–229

Turner D P, Ritts W D, Cohen W B, Maeirsperger T K, Gower S T, Kirschbaum A A, Running S W, Zhao M, Wofsy S C, Dunn A L, Law B E, Campbell J L, Oechel W C, Kwon H J, Meyers T P, Small E E, Kurc S A, Gamon J A (2005). Site-level evaluation of satellite-based global terrestrial gross primary production and net primary production monitoring. Glob Change Biol, 11(4): 666–684

Vose J M, Bolstad P V (2007). Biotic and abiotic factors regulating forest floor CO_2 flux across a range of forest age classes in the southern Appalachians. Pedobiologia (Jena), 50(6): 577–587

Wang R, Sun Q, Wang Y, Liu Q, Du L, Zhao M, Gao X, Hu Y, Guo S (2017). Temperature sensitivity of soil respiration: synthetic effects of nitrogen and phosphorus fertilization on Chinese Loess Plateau. Sci Total Environ, 574: 1665–1673

Wang X X, Sun T, Zhu Q J, Liu X, Gao F F, Hu Y M, Chen S H (2014). Assessment of different methods for estimating forest leaf area index from remote sensing data. Acta Ecol Sin, 34(16): 4612–4619 (in Chinese)

Wang Z J, Jiao J Y, Rayburg S, Wang Q L, Su Y (2016). Soil erosion resistance of "Grain for Green" vegetation types under extreme rainfall conditions on the Loess Plateau, China. Catena, 141: 109–116

Wen Z M, Brian G L, Jiao F, Lei W N, Shi H J (2010). Stratified vegetation cover index: a new way to assess vegetation impact on soil erosion. Catena, 83(1): 87–93

Wischmeier W H, Smith D D (1978). Predicting Rainfall Erosion Losses: A Guide to Conservation Planning. Washington D C: US Department of Agriculture

Xie Q Y, Dash J, Huang W J, Peng D L, Qin Q M, Mortimer H, Casa R, Pignatti S, Laneve G, Pascucci S, Dong Y Y, Ye H C (2018). Vegetation indices combining the red and red-edge spectral information for leaf Area index retrieval. IEEE J-stars, 11(5): 1482–1493

Xu H Q, Hu X J, Guan H D, Zhang B B, Wang M Y, Chen S M, Chen M H (2019). A remote sensing based method to detect soil erosion in forests. Remote Sens, 11(5): 513

Yao X, Yu K Y, Wang G Y, Deng Y B, Lai Z J, Chen Y, Jiang Y S, Liu J (2019). Effects of soil erosion and reforestation on soil respiration, organic carbon and nitrogen stocks in an eroded area of southern China. Sci Total Environ, 683: 98–108

Yu K Y, Yao X, Deng Y B, Lai Z J, Lin L C, Liu J (2019). Effects of stand age on soil respiration in Pinus massoniana plantations in the hilly red soil region of southern China. Catena, 178: 313–321

Yuan S, Zheng Y H, Wu S B, Xu P, Zhang F F, Kong F X, Qi Y D, Wang D (2018). March SST reconstruction in the South China Sea based on Pinus massoniana tree-ring widths from Changting, Fujian, in southeast China since 1893 CE. Mar Micropaleontol, 145: 21–27

Yu Z P, Wan X H, Hu Z H (2014). Contrasting responses of soil respiration to litter manipulation in subtropical Mytilaria laosensis and Cunninghamia lanceolata plantations. Acta Ecol Sin, 34: 2529–2538 (in Chinese)

Zhang C, Xie G, Liu C, Lu C (2011). Assessment of soil erosion under woodlands using USLE in China. Front Earth Sci, 5(2): 150–161

Zhang H, Yu D, Dong L, Shi X, Warner E, Gu Z, Sun J (2014 a). Regional soil erosion assessment from remote sensing data in rehabilitated high density canopy forests of southern China. Catena, 123: 106–112

Zhang Y J, Gan Z T, Li R J, Wang R, Li N N, Zhao M, Du L L, Guo S L, Jiang J S, Wang Z Q (2016). Litter production rates and soil moisture influences interannual variability in litter respiration in the semi-arid Loess Plateau, China. J Arid Environ, 125: 43–51

Zhang Y L, Song C H, Zhang K R, Cheng X L, Band L E, Zhang Q F (2014 b). Effects of land use/land cover and climate changes on terrestrial net primary productivity in the Yangtze River Basin, China, from 2001 to 2010. J Geophys Res Biogeosci, 119(6): 1092–1109

Zheng H, Chen F L, Ouyang Z Y, Tu N M, Xu W H, Wang X K, Miao H, Li X Q, Tian Y X (2008). Impacts of reforestation approaches on runoff control in the hilly red soil region of Southern China. J Hydrol (Amst), 356(1–2): 174–184

Zhou T, Shi P J, Luo J Y, Shao Z Y (2007). Estimation of soil organic carbon based on remote sensing and process model. Journal of Remote Sensing, 11(1): 127–136 (in Chinese)